

PAPER

Supercontinuum-illumination for long-workingdistance microscopic imaging of air–liquid mixed sprays in the near-nozzle region

To cite this article: Zhenqiang Huang et al 2021 Laser Phys. 31 075301

View the article online for updates and enhancements.

You may also like

- Correlations between the two-phase gas/liquid spray atomization and the Stokes/aerodynamic Weber numbers Mohammad A Rahman, Ted Heidrick and Brian A Fleck
- Assessment of steady VOF RANS turbulence models in rendering the internal flow structure of pressure swirl nozzles F Vashahi, R A Dafsari, Sh Rezaei et al.
- Long-working-distance microscopic imaging through a scattering medium using supercontinuum illumination Zhe Zhao, Wenjiang Tan, Yipeng Zheng et al

IOP Publishing | Astro Ltd Laser Physics

Laser Phys. 31 (2021) 075301 (5pp)

https://doi.org/10.1088/1555-6611/abfe53

Supercontinuum-illumination for long-working-distance microscopic imaging of air-liquid mixed sprays in the near-nozzle region

Zhenqiang Huang, Wenjiang Tan*, Jinhai Si, Shijia Zeng and Xun Hou

Key Laboratory for Physical Electronics and Devices of the Ministry of Education, Shannxi Key Lab of Information Photonic Technique, School of Electronic Science and Engineering, Xi'an Jiaotong University, Xi'an, Shaanxi 710049, People's Republic of China

E-mail: tanwenjiang@mail.xjtu.edu.cn

Received 22 October 2020 Accepted for publication 22 April 2021 Published 26 May 2021



Abstract

We demonstrate the optical diagnosis of air-liquid mixed sprays in the near-nozzle region using the supercontinuum (SC)-illumination long-working-distance microscopic imaging method, enabling the imaging of microdroplets, ligament structures, and cavities. In addition, SC-illumination long-working-distance microscopic imaging effectively suppresses speckles and reveals the ligament structures in the sprays more accurately. Finally, analysis of the droplet size distribution of the sprays under different air and liquid flow rates indicates that SC-illumination long-working-distance microscopic imaging offers several advantages for studying spray dynamics at the small structure level.

Keywords: supercontinuum, air-liquid mixed sprays, femtosecond laser, microscopic imaging

(Some figures may appear in color only in the online journal)

1. Introduction

The use of liquid fuels has become the default in many kinds of engines owing to their higher volumetric energy density and advantages they offer with respect to storage and transportation [1–3]. The growing demand for increased fuel efficiency and vehicle emission reductions is driving efforts to improve the combustion process in engines. The injection and mixing of fuel to create an efficient air phase reaction are the crucial steps of the combustion process upon which research is being focused [4–6]. To understand the factors influencing this process, lots of noninvasive optical imaging approaches have been proposed to study fuel sprays naturally, such as laser-induced fluorescence [7], laser Doppler velocimetry [8], and Raman spectroscopy [9].

However, these techniques are not always available for imaging certain dense fuel sprays, especially the near-nozzle region of the sprays, because dense fuel sprays involve a highspeed optically impenetrable two-phase flow. Many droplets, cavities, ligaments, and high-velocity bridges exist in fuel sprays at high velocities. Because of the extremely high-speed structures of the fuel sprays, images captured by diagnostic systems that use high-speed cameras to record these moving targets are affected by blurring owing to insufficiently fast exposure times. To resolve this problem, the use of ultrafast lasers as lighting sources has been suggested [10-13]. However, the incident imaging photons are susceptible to strong scattering by the dense droplet cloud, leading to the formation of speckles. These speckles corrupt the identifiability of spray features [14]. To mitigate speckle artifacts, a simple and useful approach is to use an incoherent light source to preclude speckle formation. Several studies have been devoted

^{*} Author to whom any correspondence should be addressed.

to this issue. For example, Redding et al succeeded in suppressing speckle using a low-spatial-coherence electricallypumped semiconductor laser [15]. Similarly, Cao et al used random lasers with low spatial coherences to produce specklefree images and were able to identify objects hidden under intense optical scattering conditions [16]. Barredo-Zuriarrain et al also proved the Nd doped random laser sources having the reliability for speckle-free transmission and reflection infrared imaging [17]. Some traditional incoherent light sources, such as thermal sources and light-emitting diodes, can also provide speckle-free imaging. Nevertheless, they lack sufficient intensity for imaging dense fuel sprays. Recently, Purwar et al proposed a collinear optical Kerr gate using supercontinuum (SC) to suppress the artifacts because of its coherence degeneration short pulse duration [18]. In addition, SC-illumination-based direct imaging was used to study the structures in the spray [19, 20].

However, SC-illumination-based direct imaging system could only resolve macroscopic objects with sizes greater than tens of micrometers [19]. However, the small structures with sizes of several micrometers present during early spray development, such as the air-liquid interface, ligament size, and small voids in the near-nozzle region, are crucial in determining the characteristics of the final spray. In order to elucidate spray dynamics at the small structure level, we designed an SC-illumination long-working-distance microscopic imaging system with an imaging resolution of several microns [21]. Moreover, this imaging system provides a long working distance of tens of centimeters to avoid contaminating or damaging optical elements as a result of the high temperature and pressure of the fuel sprays in the near-nozzle region [22].

In this paper, we demonstrate the optical diagnosis of air-liquid mixed sprays in the near-nozzle region using the SC-illumination long-working-distance microscopic imaging method. The results show that an 800 nm femtosecond-laserillumination microscopic imaging system can indeed observe structures with dimensions measuring several microns, such as cavities and ligaments, without incurring the blurring effects typically associated with imaging these high-speed structures. However, there are some false results in these imaging results due to the influence of speckle, such as indistinguishable ligament structures, eroded droplet boundaries, and undetectable cavities within larger liquid structures. In addition, although the SC-illumination direct imaging system can obtain lowspeckle results, there are some indistinguishable blurry spray structure boundaries and some smaller ligaments and cavities in the liquid structures because of the low spatial resolution. Nevertheless, SC-illumination long-working-distance microscopic imaging can effectively suppress speckles and distinguish ligament structures, such as cavities and droplets, with enhanced accuracy, which is very useful for analyzing spray macrodynamics. Furthermore, our analysis of droplet size distributions for sprays under different air:liquid ratios demonstrates the ability of the system to reveal spray microdynamics.

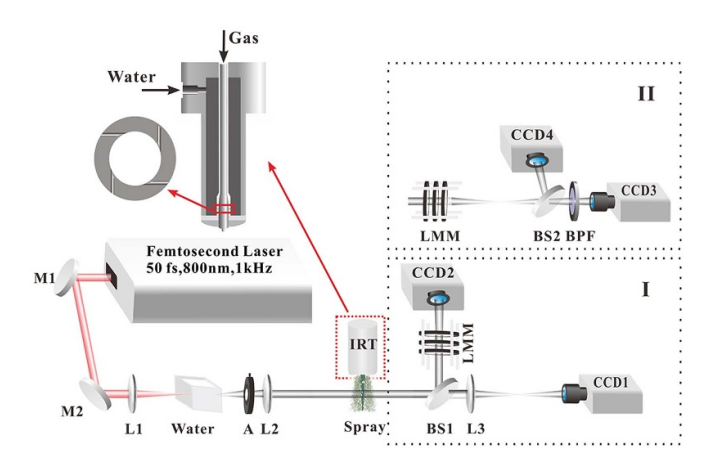


Figure 1. Experimental setup of the SC-illumination microscopic imaging system. M1, M2: reflectors; L1, L2, L3: lenses; A: aperture; LMIU: long-working-distance microscopic imaging module; BS1, BS2: beam splitters; BPF: band-pass filter; IRT: imitative rocket injector.

2. Experimental details

The experimental setup is shown in figure 1. A femtosecond laser system producing 800 nm, 3.5 mJ, 50 fs pulses at a repetition rate of 1 kHz served as the light source in the experiments. The femtosecond laser pulses were focused by lens L1 (focal length: $f_1 = 15$ cm) into a 5 cm thick quartz cuvette filled with distilled water. The SC was generated in the water upon irradiation by the femtosecond laser pulses. The intensity of the SC should be large enough to illuminate the sprays and carry the property information of these structures. Meanwhile, some neutral-density filters were introduced in front of the cameras to avoid overexposure. An aperture was used to filter the conical emission of the SC. Lens L2 (focal length: $f_2 = 15$ cm) was used to collect and collimate the SC. The collimated SC was transmitted through the near-nozzle region of the sprays to provide the imaging light. Two imaging modules were then used to study the differences in spray diagnostics for different imaging methods. Four charge-coupled device cameras (CCDs, INFINITY3-1M-NS-TPM, Lumenera Corporation, Ottawa, Canada) were used to record the images.

In imaging module I, SC-illumination long-working-distance microscopic imaging and SC-illumination direct imaging were compared. Here, the SC was divided into two parts. The transmitted part passed through lens L3 and was imaged onto CCD1 to obtain the direct images. In contrast, the reflective part was introduced into the long-working-distance microscopic imaging unit (LMIU) and imaged onto CCD2 to obtain the microscopic images. Here, we do not get rid of the fundamental laser wavelength of 800 nm. Because the low coherence of the SC containing the fundamental laser has been confirmed by our previous work [20]. On the other hand, our imaging system has a better ability to apply in highly turbid medium because of more intense incident probe light. Imaging module II was used to compare the microscopic imaging

performances using the SC and the 800 nm femtosecond laser as illumination sources. After passing through the sprays, the SC entered the LMIU and was split by a beam splitter. The transmitted part was filtered by a BPF, producing an 800 nm fundamental femtosecond laser beam. This 800 nm femtosecond laser provided the illumination for microscopic images, which were recorded by CCD3. The reflective part was imaged directly onto CCD4 to obtain SC-illumination long-working-distance microscopic images. All CCDs used an exposure time of 0.5 ms to ensure single-shot imaging in our experiment.

The sprays were generated by a home-built IRT. The schematic diagram of the IRT is show in figure 1. The liquid flow settings ranged from 0.2 to 6 l min⁻¹ with $\pm 2.5\%$ full-scale accuracy. The air flow settings ranged from 10 to $200 \ l \ min^{-1}$ with $\pm 2\%$ full-scale accuracy. The nozzle was modified from an air-centered swirl coaxial injector [23]. After filling the chamber with water, water was injected via four small passages, which were at tangents to the central axis of the cavity, into an internal cavity along the inner diameter of the nozzle. The air was pressed into the center of the nozzle by an air compressor, then flowed through the center of the nozzle and forced the liquid layer along the wall to exit the nozzle. The liquid sheet began to break up and formed airliquid mixed sprays at the exit lip of the injector. The acquisition time of each image is about 1 s. We can get three or four images in each spray process, which is limited by the holding time of constant air pressure and liquid pressure of our experimental setup.

3. Results and discussion

First, a resolution test target (RT, RT-MIL-TP2001, Beijing RealLight Technology Co., Ltd, China) was imaged to evaluate the performance of our imaging system. The contrast-to-noise ratio (CNR) curves of each experimental configuration were calculated and are shown in figure 2. The CNR represents the identifiability of a feature of interest against a given background, as shown in figure 2. The CNR value was calculated using equation (1):

$$CNR = (\langle I_{A} \rangle - \langle I_{B} \rangle) / [(\sigma_{A} + \sigma_{B}) / 2]$$
 (1)

where $I_{\rm A}$ and $I_{\rm B}$ are the intensities of signal-producing structures A and B, respectively, in the region of interest. In our results, A and B are the bars in a test pattern and the surrounding background, respectively, and σ is the standard deviation of the pixel intensity. The structures are unidentifiable when the CNR is <1. We calculated each data point in the CNR curves five times to get the mean values and the corresponding standard errors. The results were shown in figure 2. Figure 2 shows the spatial resolutions of the different imaging methods. We can see that the spatial resolutions are approximately 10.8, 4.1, and 4.1 μ m for the SC-illumination direct imaging, 800 nm femtosecond-laser-illumination microscopic imaging, and SC-illumination microscopic imaging systems, respectively, in the absence of scattering disturbance. However, the spatial resolution of the

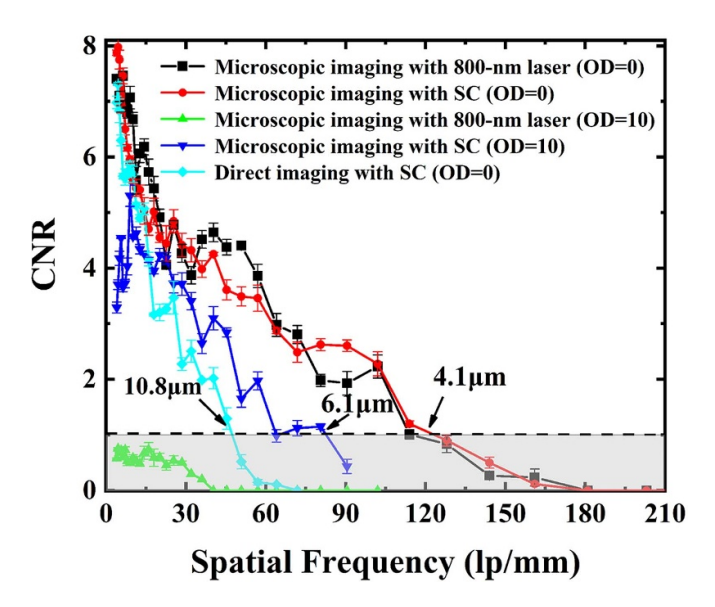


Figure 2. CNR results for the SC-illumination direct imaging, 800 nm femtosecond-laser-illumination microscopic imaging, and SC-illumination microscopic imaging systems in different scattering conditions (i.e. for OD = 0 and OD = 10). The horizontal dashed black line represents a CNR value of 1, with the gray-shaded region indicates the structures are unidentifiable. The unit of x-axis is line pairs per millimeter (lp mm⁻¹).

800 nm femtosecond-laser-illumination microscopic imaging system seriously degrades when the imaging target is hidden in environments with strong scattering. As shown in figure 2, the CNR of this imaging system decreases to approximately 0.8 at OD \approx 10. Here, OD is defined as OD = $-\ln(I/I_0)$, where I is the irradiance of light exiting the scattering medium and I_0 is the irradiance of light entering the scattering medium. By contrast, the spatial resolution of the SC-illumination microscopic images decreased to approximately 6.1 μ m at OD \approx 10. In fact, our main goal is suppressing the speckle using SC, the image resolution and contrast of images obtained through SC-illumination long-working-distance microscopic imaging are both significantly improved. However, the chromatic aberration was also introduced when we used the SC to image the spray in our experiment. The imaging resolution might be improved further if the achromatic lens was used.

Next, we compared the performance of the two SCillumination imaging methods with respect to diagnosing the air-liquid mixed sprays. The air and liquid flow rates were 190 and 0.4 l min⁻¹, respectively. Figures 3(a) and (b) show images of the air-liquid mixed sprays captured using SC-illumination direct imaging and SC-illumination microscopic imaging, respectively. The image labels I, II, and III in figure 3 represent images captured at the same position at different intervals. In figure 3(a), we can see some small spray structures, including ligaments, cavities, and droplets, are captured in the SC-illumination direct images as a result of freezing the motion of the spray structure. However, in the magnified insets, we can see that boundaries of the spray structures, including some smaller ligaments and cavities, are blurred and indistinguishable because of the low spatial resolution. Figure 3(b) shows the same structures captured

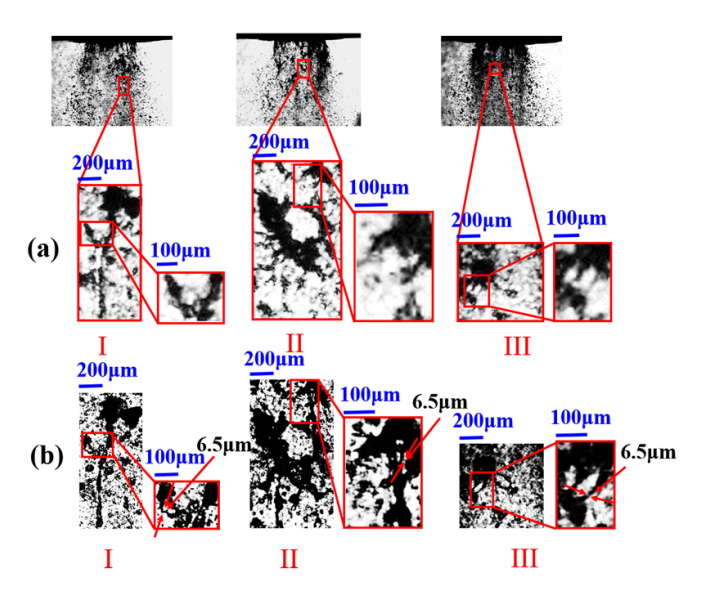


Figure 3. Images of air–liquid sprays obtained by (a) SC-illumination direct imaging and (b) SC-illumination microscopic imaging with enlargements of the red-bounded regions. The air and liquid flow rates were 190 and 0.4 1 min⁻¹, respectively.

by SC-illumination long-working-distance microscopic imaging revealing conspicuously sharper structure edges, with the structures enlarged in the insets far easier to discern than in figure 3(a). For example, in figure 3(b)-I we can identify a 6.5 μ m ligament structure and an authentic cavity near the ligament, which cannot be distinguished in figure 3(a)-I. Similar observations are evident from comparing images II and III acquired via the two methods. These results indicate that many smaller structures can be imaged at a useful resolution via SC-illumination long-working-distance microscopic imaging, which will be beneficial for studying spray dynamics.

Then, two microscopic imaging methods using the 800 nm femtosecond laser and the SC were compared. The air and liquid flow rates are 160 and 0.4 1 min^{-1} , respectively. Figures 4(a) and (b) show the images of the air-liquid mixed sprays captured by 800 nm femtosecond-laser-illumination microscopic imaging and SC-illumination long-workingdistance microscopic imaging, respectively. In each case, images I, II, and III represent images captured at the same position at different intervals. In figure 4(a), we can distinguish some small structures, such as small droplets, ligaments, and cavities in the liquid structure, owing to the high imaging resolution and the spray structures being frozen by using 800 nm femtosecond-laser-illumination microscopic imaging. However, from the magnified regions in figure 4(a), it is clear that the boundaries of the droplets and ligaments are blurred because of speckle erosion. In addition, some finer cavities in the liquid structures are also unidentifiable. Figure 4(b) shows the same structures captured by SC-illumination long-working-distance microscopic imaging. In this case, we can see that the boundaries of the droplets and ligaments with greater clarity, while speckle suppression enhances the accurate identification of small cavities in the liquid structure. For example, we can see that the boundaries of the droplets are sharper in figure 4(b)-I relative to figure 4(a)-I.

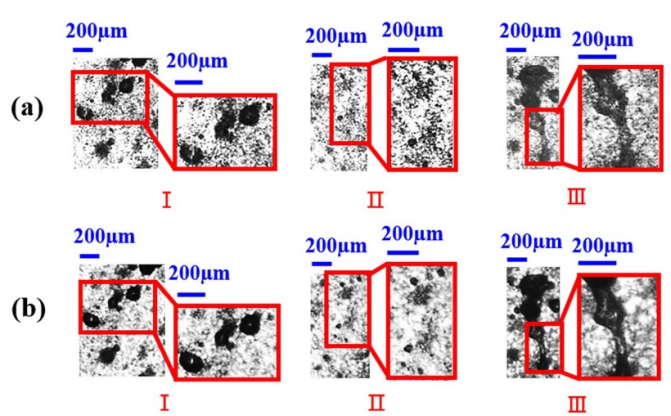


Figure 4. Images of air–liquid sprays obtained by (a) 800 nm femtosecond-laser-illumination microscopic imaging and (b) SC-illumination microscopic imaging with enlargements of the red-bounded regions. The air and liquid flow rates were 160 and $0.4 \, 1 \, \mathrm{min}^{-1}$, respectively.

Moreover, some of the small droplets and cavities observed in figures 4(b)-II and III are indistinguishable in figures 4(a)-II and III. Because SC-illumination long-working-distance microscopic imaging can suppress speckles effectively and identify small structures with greater reliability, it provides more information-rich images for the study of spray dynamics at the micrometer scale.

Finally, we applied the SC-illumination long-workingdistance microscopic imaging method to study the droplet size distribution in the near-nozzle region of the air-liquid mixed sprays for different air and liquid flow rates. The liquid flow rate was varied from 0.2 to 0.6 1 min⁻¹, while the air flow rate was varied from 100 to 190 l min⁻¹. To reveal the statistical characteristics of the droplet size distribution for different operating conditions, In order to reveal the statistical characteristics of the droplet size distribution for different operating conditions, 40 spray images with five groups were captured for one operating condition. The percentage of droplets was calculated by the ratio of the droplet number in a fixed particle size range and the total droplet number in each group. Here, we set the fixed particle size range into 3 μ m. Finally, we got five independent droplet size distributions data for each condition. We found that the droplet size distribution is almost unchanged for different groups of spray image in one operating condition. So an average droplet size distribution curve was calculated to represent the statistical characteristics of sprays. The errors were also calculated form the five independent groups of data. The results were shown in figure 5. A resolution test target (RT, RT-MIL-TP2001, Beijing RealLight Technology Co., Ltd, China) was imaged to obtain the scale for all the spray images. Then the droplet size in each image was obtain manually. Finally, the mean values and standard errors were calculated form the five independent droplet size distributions data for each condition. The results were shown in figure 5. From the results, we can see that the droplet size ranges from a few microns to more than 70 microns in our experiments. In addition, the median droplet size became smaller as the air flow rate was increased, while maintaining a fixed liquid flow rate. For example, when the liquid flow rate was set at

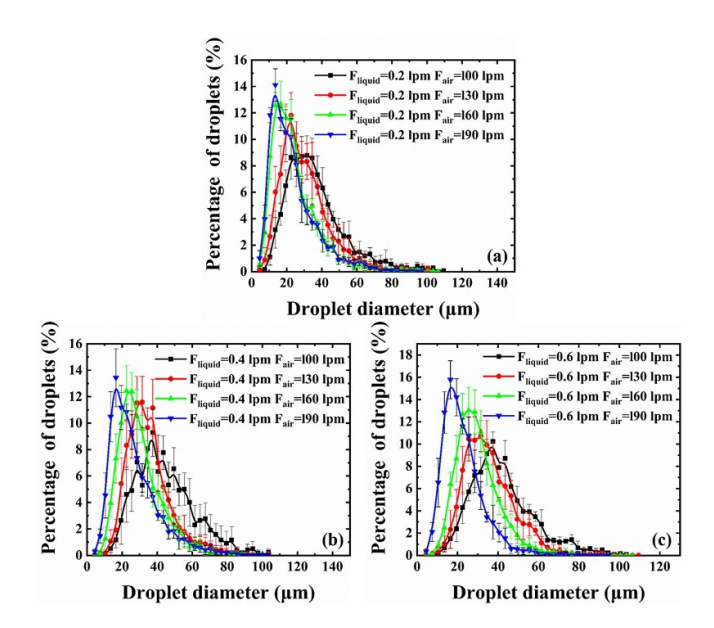


Figure 5. Droplet size distributions for different air–liquid ratios. F_{liquid} —liquid flow rate; F_{air} —air flow rate.

 $0.61 \,\mathrm{min^{-1}}$, as shown in figure 5(a), the median droplet size changed from approximately 36 μ m to sizes of 30, 20, and 15 μ m as the air flow rate changed from 100 to 130, 160, and $190 \,\mathrm{l}\,\mathrm{min}^{-1}$, respectively. Moreover, the distribution range of droplet sizes also decreased as the air flow rate was increased for a fixed liquid flow rate. This is because the atomization of sprays is more sufficient with a higher air flow rate at a fixed liquid flow rate. Nevertheless, we also see that the range of the diameter of the droplets remains approximately invariant to decreasing liquid flow rate for a fixed air flow rate. We attribute this phenomenon to the fact that the air flow rate is much higher than the liquid flow rate and, therefore, exerts more influence on the atomization of the sprays in our experiment. These results demonstrate the ability of our SCillumination microscopic imaging system to elucidate spray microdynamics.

4. Conclusion

In conclusion, SC-illumination long-working-distance microscopic imaging, 800 nm femtosecond-laser-illumination microscopic imaging, and SC-illumination direct imaging were compared for the imaging of air-liquid mixed sprays. The results show that small structures were captured with conspicuously sharper edges owing to the improved resolution provided by SC-illumination long-working-distance microscopic imaging compared to SC-illumination direct imaging. Consequently, SC-illumination long-working-distance microscopic imaging enabled small spray structures to be identified with greater confidence owing to the suppression of speckles and an improved spatial resolution compared to 800 nm femtosecond-laser-illumination microscopic imaging. Moreover, we applied the SC-illumination long-workingdistance microscopic imaging method to analyze the droplet size distribution in the near-nozzle region of the air-liquid mixed sprays for different air and liquid flow rates. Droplets with sizes ranging from several microns to tens of microns were imaged. In addition, the median droplet size decreased with increasing air flow rate when the liquid flow rate was maintained at a fixed value. The results demonstrate the ability of SC-illumination long-working-distance microscopic imaging to provide important information to provide new insights into spray dynamics at the micrometer scale.

Acknowledgments

This study was supported by grants from the National Natural Science Foundation of China (NSFC) (62027822, 61690221), the National Key Research and Development Program of China (2019YFA0706402), the Natural Science Basic Research Plan in Shaanxi Province of China (2018JM6012), and the Fundamental Research Funds for the Central Universities (xzy012019039).

References

- [1] Chu S and Majumdar A 2012 Nature 488 294
- [2] Fischer M, Werber M and Schwartz P V 2009 Energy Policy 37 2639
- [3] Chu S 2008 AIP Conf. Proc. 1044 266
- [4] Jarrahbashi D, Sirignano W A, Popov P P and Hussain F 2016 J. Fluid Mech. 792 186
- [5] Wang Z, Ding H, Ma X, Xu H and Wyszynski M L 2016 J. Appl. Energy 163 105
- [6] Moon S, Gao Y, Wang J, Fezzaa K and Tsujimura T 2014 Fuel 133 299
- [7] Mulla I A, Dowlut A, Hussain T, Nikolaou Z M, Chakravarthy S R, Swaminathan N and Balachandran R 2016 Combust. Flame 165 373
- [8] Soid S N and Zainal Z A 2011 Energy 36 724
- [9] Correia Rodrigues H, Tummers M J, van Veen E H and Roekaerts D J E M 2015 Combust. Flame 162 759
- [10] Wu Z, Zhu Z and Huang Z 2006 Fuel 85 1458
- [11] Crua C, Heikal M R and Gold M R 2015 Fuel 157 140
- [12] Fansler T D and Parrish S E 2015 *Meas. Sci. Technol.* **26** 012002
- [13] Purwar H, Wang H, Tang M, Idlahcen S, Rozé C, Blaisot J, Godin T and Hideur A 2015 Opt. Express 23 33396
- [14] Gaska J P, Tai C F and Geri G A 2007 J. Soc. Inf. Disp. 15 1023
- [15] Redding B, Cerjan A, Huang X, Lee M L, Stone A D, Choma M A and Cao H 2015 Proc. Natl Acad. Sci. USA 112 1304
- [16] Redding B, Choma M A and Cao H 2012 Nat. Photon. 6 355
- [17] Barredo-Zuriarrain M, Iparraguirre I, Fernández J, Azkargorta J and Balda R 2017 Laser Phys. Lett. 14 106201
- [18] Purwar H, Idlahcen S, Rozé C and Blaisot J B 2015 (available at: https://arxiv.org/abs/1502.07255)
- [19] Zheng Y, Si J, Tan W, Ren Y, Tong J and Hou X 2016 Opt. Express 24 26338
- [20] Zheng Y, Si J, Tan W, Wang M, Yang B and Hou X 2018 Opt. Eng. 57 043114
- [21] Zhao Z, Tan W, Zheng Y, Wang M and Liu X 2019 Phys. Scr. 94 045505
- [22] Sjöberg H, Manneberg G and Cronhjort A 1996 Opt. Eng. 35 3591
- [23] Cheng G C, Cohn R, Johnson C, Davis R R and Muss J A 2003 39th AIAA/ASME/SAE/ASEE Joint Propulsion Conf. and Exhibit (Aerospace Research Central) paper 4751 (https://doi.org/10.2514/6.2003-124)